

# Dalton Transactions

Accepted Manuscript



This is an *Accepted Manuscript*, which has been through the RSC Publishing peer review process and has been accepted for publication.

*Accepted Manuscripts* are published online shortly after acceptance, which is prior to technical editing, formatting and proof reading. This free service from RSC Publishing allows authors to make their results available to the community, in citable form, before publication of the edited article. This *Accepted Manuscript* will be replaced by the edited and formatted *Advance Article* as soon as this is available.

To cite this manuscript please use its permanent Digital Object Identifier (DOI®), which is identical for all formats of publication.

More information about *Accepted Manuscripts* can be found in the [Information for Authors](#).

Please note that technical editing may introduce minor changes to the text and/or graphics contained in the manuscript submitted by the author(s) which may alter content, and that the standard [Terms & Conditions](#) and the [ethical guidelines](#) that apply to the journal are still applicable. In no event shall the RSC be held responsible for any errors or omissions in these *Accepted Manuscript* manuscripts or any consequences arising from the use of any information contained in them.

Cite this: DOI: 10.1039/c0xx00000x

www.rsc.org/xxxxxx

Paper

# One-step replication and enhanced catalytic activity for cathodic oxygen reduction of the mesostructured Co<sub>3</sub>O<sub>4</sub>/Carbon composites

Yongxia Wang,<sup>a,b</sup> Xiangzhi Cui,<sup>b</sup> Lisong Chen,<sup>b</sup> Chenyang Wei,<sup>b</sup> Fangming Cui,<sup>c</sup> Heliang Yao,<sup>b</sup> Jianlin Shi<sup>\*b</sup>, Yongsheng Li<sup>\*a</sup>

Received (in XXX, XXX) Xth XXXXXXXXX 20XX, Accepted Xth XXXXXXXXX 20XX

DOI: 10.1039/b000000x

Mesostructured Co<sub>3</sub>O<sub>4</sub>/C composites of high surface areas have been synthesized via a one-step replica route by co-nanocasting cobalt and carbon precursors into mesoporous silica, in which the Co<sub>3</sub>O<sub>4</sub> nanoparticles are homogeneously dispersed in the mesoporous structure of carbon substrates. The mesostructured composites showed relatively high catalytic activities for oxygen reduction reaction (ORR), and that with a Co loading content of 4.3 at% exhibited the best electrochemical performance for ORR. The relatively high catalytic activity is attributed to the effects of the redox couples (Co<sup>3+</sup>/Co<sup>2+</sup>) together with the contribution from the conductive mesoporous carbon substrate.

## Introduction

Oxygen reduction reaction (ORR) is one of the fundamental reactions taking place on the cathode catalytic surface of H<sub>2</sub>-O<sub>2</sub> fuel cells,<sup>1, 2</sup> such as proton exchange membrane fuel cells (PEMFCs), which is so important that numerous efforts have been devoted to developing high performance while cost-effective cathode catalysts for ORR. Unfortunately, the present cathode catalysts in PEMFCs still faces a number of problems and challenges. On one hand, compared with a rather fast oxidization of hydrogen that produces proton and electron at the anode, the sluggish ORR is a main challenge for developing fuel cells of high enough performance and efficiency for commercial applications. On the other hand, the high cost and limited supply of the precious Pt-based catalysts, the most successful electrocatalysts for ORR up to now, greatly hinder their large-scale commercial applications.<sup>3</sup> Consequently, it is highly desirable to develop highly active cathode catalysts with as low as possible Pt using amount or even non-precious metal catalysts. Hashyam and Lefèvre et al. are the pioneers in developing fuel cell technology using non-precious metal catalysts for ORR,<sup>4, 5</sup> which has aroused great interest in searching novel, highly active and stable non-precious metal catalysts over the past decades,<sup>6-9</sup> in particular the non-precious metal-containing carbon nanostructured catalysts for ORR.<sup>10-13</sup>

Among the non-precious metal electro-catalysts for ORR, Co<sub>3</sub>O<sub>4</sub> has been widely investigated as the alternative catalysts in terms of their low cost, moderate electrical resistance and environmental friendliness, which demonstrates promising catalytic activity and durability in alkaline or acidic media.<sup>14-17</sup> However, Co<sub>3</sub>O<sub>4</sub> is p-type semiconductor, and the use of conductive substrates is necessary to elevate the electron conductivity and improve the electrochemical properties for ORR, among which, carbonaceous materials have been suggested

as possible electrocatalyst supports attributing to their high mechanical strength, excellent electronic conductivity as well as chemical stability, such as Vulcan XC72, carbon nanotubes, graphene, mesoporous carbon, and so on.<sup>18-23</sup>

Mesoporous materials have been paid much attention in various application fields, such as catalysis, fine chemical engineering, drug delivery system, separation and adsorption, thanks to their high specific surface areas, pore volumes, controlled pore sizes and size distributions in their extensive mesoporosities, and so on.<sup>24-28</sup> The interconnected pore network of the mesoporous carbon benefits the diffusion of ORR-related molecules and dispersion of guest species, while the carbonaceous framework plays a role of electron conduction during ORR, both of which favors the enhancement of the electrochemical catalytic activity. However, up to now, the reported methodologies of preparing Co<sub>3</sub>O<sub>4</sub>/C composites were relatively complicated, which mainly involved two major steps of the carbon preparation with varied morphologies and the post-loading of the Co<sub>3</sub>O<sub>4</sub> nanoparticles onto/into pre-obtained carbonaceous substrates.<sup>18, 29-31</sup> Additionally, no reports can be found on the synthesis and the ORR performances of the mesostructured Co<sub>3</sub>O<sub>4</sub>/C composites prepared by a one step process. Herein, we demonstrate the synthesis of a mesostructured Co<sub>3</sub>O<sub>4</sub>/C composite via a simple one-step replication route in which cobalt and carbon precursors were co-nanocasted into the pore network of a mesoporous silica template. The resultant composites show homogeneous dispersion of Co<sub>3</sub>O<sub>4</sub> nanoparticles in mesoporous network of the carbon substrates, and highly efficient performances in ORR.

## Experimental

**Synthesis of mesostructured Co<sub>3</sub>O<sub>4</sub>/C composites.** The as-prepared mesoporous silica (KIT-6) following the procedure reported by R. Ryoo et al.<sup>32</sup> were used as a hard template for the

preparation of mesostructured  $\text{Co}_3\text{O}_4/\text{C}$  composites. The typical synthesis procedure is as follows: Different amounts of cobaltous acetate ( $\text{Co}(\text{C}_2\text{H}_3\text{O}_2)_2$ ) and 1.5 mL furfuralcohol were dissolved in ethanol solvent. The above mixed solution was co-casted into 1.0 g as-prepared KIT-6 by a wetness impregnation technique. After the solvent evaporated, the precursors@silica composite was calcined at 1023 K for 4 h with heating rate of  $2 \text{ K min}^{-1}$  in pure  $\text{N}_2$ . The silica template was finally removed by treating in 2 M NaOH solution at 353 K. This template-free  $\text{Co}_3\text{O}_4/\text{C}$  composites were collected by centrifugation and washed with distilled water and ethanol, and then dried at 353 K. The mesostructured  $\text{Co}_3\text{O}_4/\text{C}$  composites were named as 1- $\text{Co}_3\text{O}_4/\text{C}$ , 2- $\text{Co}_3\text{O}_4/\text{C}$  and 3- $\text{Co}_3\text{O}_4/\text{C}$ , corresponding to the Co loading amounts of 1.1, 4.3 and 11.4 at%, respectively. For comparison, the mesoporous  $\text{Co}_3\text{O}_4$  and carbon were also synthesized via the same process same to the above-described.

**Characterization.** The powder X-ray diffraction (XRD) patterns of the as-prepared samples were recorded on a Rigaku D/Max-2550V X-ray diffractometer with a Cu  $\text{K}\alpha$  radiation target (40 kV, 40 mA). The morphology of the mesostructured  $\text{Co}_3\text{O}_4/\text{C}$  composites were observed using a transmission electron microscopic (TEM) (a JEOL 200CX electron microscope operating at 160 kV). Raman spectra were recorded on Micro-Raman spectrometer (Jobin Yvon HR800 UV) using an Ar ion laser (excitation wavelength: 514.5 nm). The  $\text{N}_2$  sorption measurements were performed using Micromeritics Tristar 3000 at 77 K, and the specific surface area and pore size distributions were calculated using the Brunauer–Emmett–Teller (BET) and Barrett–Joyner–Halenda (BJH) methods, respectively.

Electrochemical experiments were performed on CHI 660E electrochemical workstation (CH Instrument, Inc.) with a standard three-electrode cell. Glassy carbon disks of 6 mm diameter ( $0.283 \text{ cm}^2$ ) served as substrate for the catalysts. Catalyst ink with  $5 \text{ mg mL}^{-1}$  (ethanol :water = 1 : 1, volume scale) and  $25 \mu\text{L}$  Nafion solution (5%) was dispersed ultrasonically, and  $20 \mu\text{L}$  aliquot was transferred onto the glassy carbon substrate, yielding a catalyst loading level of  $0.35 \text{ mg cm}^{-2}$ . A platinum wire and  $\text{Ag}/\text{AgCl}$  (3 M KCl) were used as counter and reference electrodes, respectively.  $\text{O}_2$ -saturated 0.5 M  $\text{H}_2\text{SO}_4$  solution was used as electrolyte for electrochemical measurements. The catalysts were characterized by cyclic voltammetry (CV) test at room temperature. An electrode tip (ALS, RRDE-3A Operation Manual) was used for the rotating disk electrode (RDE) measurements, and glassy carbon disks of 4 mm diameter served as substrate for the catalyst materials. The kinetic parameters can be analyzed on the basis of the Koutecky-Levich equations:

$$\frac{1}{J} = \frac{1}{J_L} + \frac{1}{J_K} = \frac{1}{B\omega^{1/2}} + \frac{1}{J_K}$$

$$B = 0.62nFC_0(D_0)^{2/3}v^{-1/6}$$

$$J_K = nFkC_0$$

In which  $J$  is the measured current density,  $J_K$  and  $J_L$  are the kinetic and diffusion-limiting current densities,  $\omega$  is the rotation rate in rpm,  $n$  is the overall number of electrons transferred in oxygen reduction,  $F$  is the Faraday constant ( $F = 96485 \text{ C mol}^{-1}$ ),  $C_0$  is the bulk concentration of  $\text{O}_2$  ( $C_0 = 1.3 \times 10^{-6} \text{ mol cm}^{-3}$ ),  $D_0$  is diffusion coefficient of  $\text{O}_2$  in the bulk solution ( $D_0 = 1.7 \times 10^{-5} \text{ cm}^2 \text{ s}^{-1}$ ),  $v$  is the kinematic viscosity of the solution ( $0.01 \text{ cm}^2 \text{ s}^{-1}$ ),  $k$  is the electron-transfer rate constant. The number of electron

transfer rate ( $n$ ) can be obtained from the slope of the Koutecky-Levich plots ( $J^{-1}$  vs  $\omega^{-1/2}$ ).

The surface and/or lattice oxygen reduction behaviors of the obtained mesostructured  $\text{Co}_3\text{O}_4/\text{C}$  composites were explored by using temperature-programmed reduction of the hydrogen ( $\text{H}_2$ -TPR) technique in a temperature range from 293 to 1073 K on the TCD-GC analyzer. Typically, 50 mg of sample placed in glass tube was first thermally treated under a He flow at 923 K for 30 min a rate of  $10 \text{ K min}^{-1}$ , and then cooled down to the room temperature. Afterward, the 10%  $\text{H}_2$  in Ar was introduced into the glass tube with a flow rate of  $25 \text{ ml min}^{-1}$  for the TPR experiment.

## Results and discussion

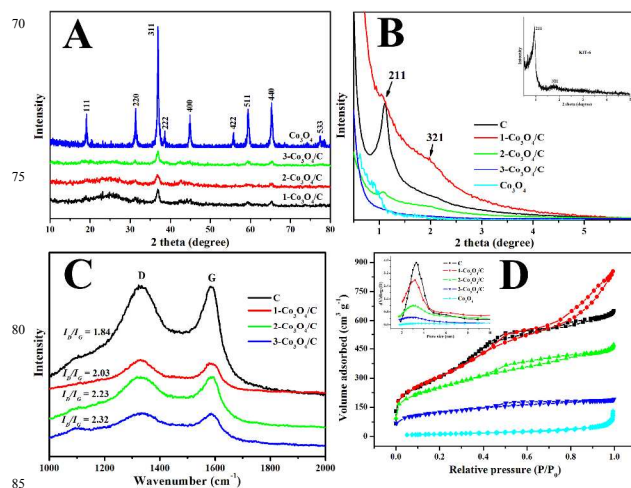


**Fig. 1** Wide-angle and small-angle XRD patterns of the mesostructured  $\text{Co}_3\text{O}_4/\text{C}$  composites (A and B), the inset in B is the small-angle XRD pattern of the silica template; Raman spectra of the composites (C);  $\text{N}_2$  sorption isotherms of the composites (D), the insets in D are corresponding BJH pore size distribution.

XRD patterns of the as-prepared mesoporous  $\text{Co}_3\text{O}_4$  and mesostructured  $\text{Co}_3\text{O}_4/\text{C}$  composites are shown in Fig. 1A, and all peaks can be well indexed to those of  $\text{Co}_3\text{O}_4$  crystalline phase (JCPDS no.: 42-1467). It can also be seen that the peak intensities of all  $\text{Co}_3\text{O}_4/\text{C}$  composites are relatively weak and broadened compared to those of the mesoporous  $\text{Co}_3\text{O}_4$ , indicating the diminished nanocrystalline size of  $\text{Co}_3\text{O}_4$  particles after loaded in the mesoporous carbon substrates. Fig. 1B and the inset give the small-angle XRD patterns of the as-prepared samples and silica template, respectively. The silica template exhibits well-resolved small angle peaks, and one characteristic diffraction peak (211) can be detected for the pure mesoporous carbon and  $\text{Co}_3\text{O}_4$ , indicating that the ordered pore structure can be reserved for the samples after silica template removal. The diffraction peaks of the  $\text{Co}_3\text{O}_4/\text{C}$  composites in the small angle region become less significant at the increased  $\text{Co}_3\text{O}_4$  loading contents, indicating that the loading of  $\text{Co}_3\text{O}_4$  nanoparticles will lead to the partial damages of the mesopore ordering of the mesoporous carbon substrate during co-nanocasting process. Moreover, the loaded  $\text{Co}_3\text{O}_4$  may affect the microstructure of the carbon substrate as shown in the Raman spectra (Fig. 1C). The spectra show two bands at 1355 (D) and 1590 (G)  $\text{cm}^{-1}$ , and the  $I_D/I_G$  of the composites increases with the increase of the  $\text{Co}_3\text{O}_4$  loading

content, attributable to the defects and disorder of the carbon after the loading of the  $\text{Co}_3\text{O}_4$ .

$\text{N}_2$  adsorption-desorption isotherms and the corresponding BJH pore size distribution curves of the obtained samples are shown in Fig. 1D. All samples show a type-IV isotherm with hysteresis loops located in the relative pressure range of 0.5 ~ 1.0, which is the characteristic of mesoporous materials. The pore structure parameters of all samples are listed in Table S1, and the specific surface area decreases gradually with the increasing loading content of  $\text{Co}_3\text{O}_4$ , while all of the as-prepared mesoporous  $\text{Co}_3\text{O}_4/\text{C}$  composites show almost identical pore size distribution (about 3 nm). The Co contents from the XPS (Fig. S1) were determined to be 1.1, 4.3 and 11.4 at%, corresponding to the as-prepared mesostructured 1- $\text{Co}_3\text{O}_4/\text{C}$ , 2- $\text{Co}_3\text{O}_4/\text{C}$ , and 3- $\text{Co}_3\text{O}_4/\text{C}$  composites, respectively.

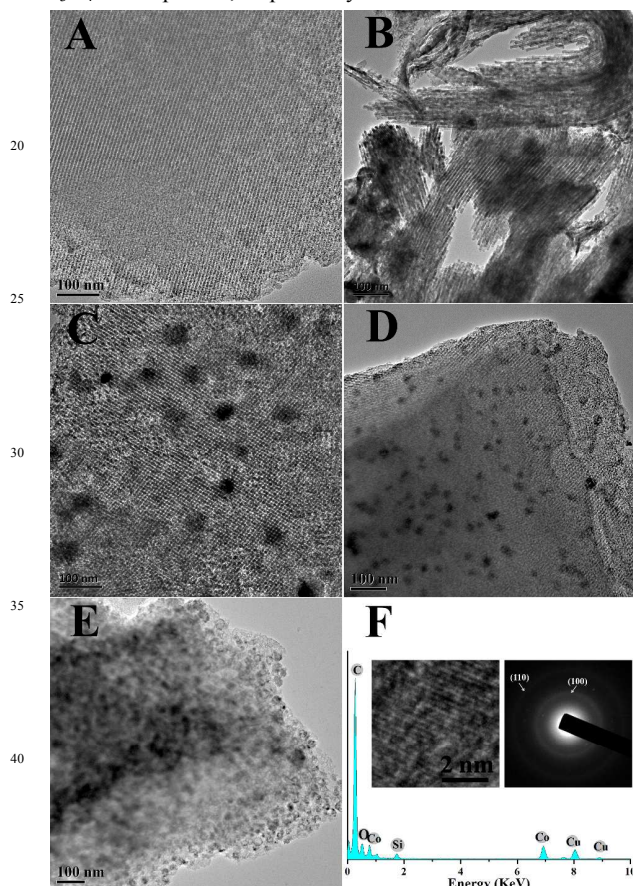


**Fig. 2** TEM images of mesoporous carbon (A),  $\text{Co}_3\text{O}_4$  (B), 1- $\text{Co}_3\text{O}_4/\text{C}$  (C), 2- $\text{Co}_3\text{O}_4/\text{C}$  (D), 3- $\text{Co}_3\text{O}_4/\text{C}$  (E); EDS pattern of mesostructured 1- $\text{Co}_3\text{O}_4/\text{C}$  (F), and the left and right insets in F are the corresponding HRTEM image and SAED pattern of the 1- $\text{Co}_3\text{O}_4/\text{C}$ .

Fig. 2A and B give the TEM images of the mesoporous carbon and  $\text{Co}_3\text{O}_4$ , respectively, and it can be seen that both of samples show ordered mesostructure after the removal of the silica template. Fig. 2C, D and E are the typical TEM images of 1- $\text{Co}_3\text{O}_4/\text{C}$ , 2- $\text{Co}_3\text{O}_4/\text{C}$ , and 3- $\text{Co}_3\text{O}_4/\text{C}$ , respectively, which shows the homogenous dispersions of  $\text{Co}_3\text{O}_4$  nanoparticles in/on the mesoporous carbon substrates. Moreover, with the increase of the  $\text{Co}_3\text{O}_4$  loading content, the pore structure ordering of the  $\text{Co}_3\text{O}_4/\text{C}$  composites is deteriorated gradually, which corresponds

to the variation of their surface areas. The EDS of the mesostructured 1- $\text{Co}_3\text{O}_4/\text{C}$  composite (Fig. 2D) also proves the successful loading of  $\text{Co}_3\text{O}_4$  in the mesoporous carbon substrates in which the signals of Co and O can be readily detected. Additionally, very weak Si signal can be distinguished, suggesting the trace amount of Si remained due to the strong interaction between silica and obtained sample as also found by others.<sup>33, 34</sup> The left inset in Fig. 2F is the HRTEM image of 1- $\text{Co}_3\text{O}_4/\text{C}$ , and the (311) plane with a lattice space of 0.244 nm is observed for  $\text{Co}_3\text{O}_4$  nanoparticles, indicating the crystalline character of  $\text{Co}_3\text{O}_4$  in mesoporous carbon substrates. Meanwhile, the selected area electron diffraction (SAED) pattern (the right inset in Fig. 2F) shows a clear evidence of a certain degree of graphitic structure of the mesoporous carbon substrates.

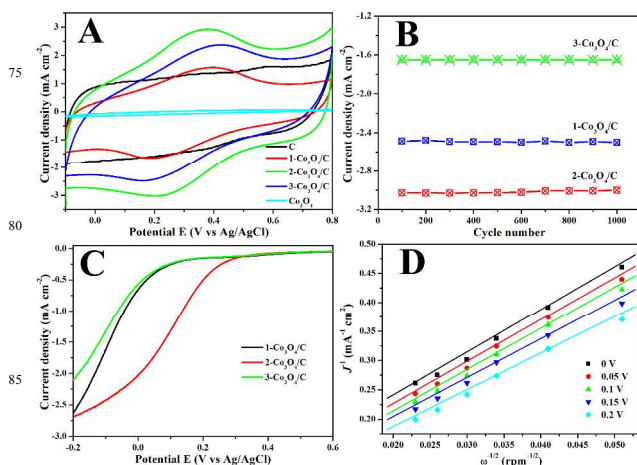


**Fig. 3** CV curves of the mesostructured  $\text{Co}_3\text{O}_4/\text{C}$  composites in  $\text{O}_2$ -saturated 0.5 M  $\text{H}_2\text{SO}_4$ ,  $\nu = 50 \text{ mV s}^{-1}$  (A); Plots of current density vs cycle number of the composites for oxygen reduction (B); RDE voltammetry curves of the composites for oxygen reduction obtained at 1600 rpm in  $\text{O}_2$ -saturated 0.5 M  $\text{H}_2\text{SO}_4$ ,  $\nu = 2 \text{ mV s}^{-1}$  (C); Koutecky-Levich plots of 2- $\text{Co}_3\text{O}_4/\text{C}$  in  $\text{O}_2$ -saturated 0.5 M  $\text{H}_2\text{SO}_4$  for oxygen reduction at varied potentials (D).

The electrochemical catalytic activities for oxygen reduction reaction (ORR) of the obtained mesostructured  $\text{Co}_3\text{O}_4/\text{C}$  composites were examined using cyclic voltammetry (CV) in  $\text{O}_2$ -saturated 0.5 M  $\text{H}_2\text{SO}_4$ . Fig. 3A gives the CV curves of the composites under scanning rate of  $50 \text{ mV s}^{-1}$ , and clear redox peaks can be observed for all of the  $\text{Co}_3\text{O}_4/\text{C}$  composites. However, the pure mesoporous  $\text{Co}_3\text{O}_4$  and pure mesoporous carbon shows no redox peaks for ORR, indicating that neither mesoporous  $\text{Co}_3\text{O}_4$  nor carbon is a satisfactory catalyst for oxygen reduction. The similar results have also been reported by Dai et al. that  $\text{Co}_3\text{O}_4$  or graphene oxide alone has little catalytic activity, while the hybrid material of  $\text{Co}_3\text{O}_4$  nanocrystals grown on reduced graphene oxide exhibits an unexpected, surprisingly high ORR activity.<sup>18</sup> Additionally, the mesostructured 2- $\text{Co}_3\text{O}_4/\text{C}$  composites (Co content of 4.3 at%) show the highest ORR catalytic performance among the mesostructured  $\text{Co}_3\text{O}_4/\text{C}$  composites. This result indicates that the moderate  $\text{Co}_3\text{O}_4$  loading favors the enhanced catalytic ORR activity of the catalysts, while over-high or over-low amounts of  $\text{Co}_3\text{O}_4$  dispersions may lead to decreased activities in ORR. Additionally, though the reduction

potential of the mesostructured 2-Co<sub>3</sub>O<sub>4</sub>/C composite (0.22 V) is lower than that of the standard E-TEK cathode catalysts 40% Pt/C (0.57 V) (Fig. S2A), the maximum reduction current density of the 2-Co<sub>3</sub>O<sub>4</sub>/C about 3.0 mA cm<sup>-2</sup> is similar to that of the Pt/C (about 2.6 mA cm<sup>-2</sup>), indicating that the mesostructured 2-Co<sub>3</sub>O<sub>4</sub>/C composite is a good catalyst candidate for ORR. The peak current of the synthesized catalysts are also higher than most of the cobalt-based catalysts [35, 36]. The Fig. 3B gives the plots of current density of the Co<sub>3</sub>O<sub>4</sub>/C composites versus the cycle number, and the current density of all the catalysts can retain their initial current densities after several hundred or even one thousand cycles, indicating the high redox cycling stability. The current density versus time curves (Fig. S2B) of the catalysts also exhibit the high ORR stability. Meanwhile, the CV curves of the mesostructured Co<sub>3</sub>O<sub>4</sub>/C composites after cycled for 1000 times for ORR are shown in Fig. S2 (C-D).

Linear sweep voltammetry with a rotating disk electrode (RDE) were further employed to study the ORR activity and kinetics of the composites. Fig. 3C shows the ORR polarization curves obtained at a rotation rate of 1600 rpm, and the onset potential for 2-Co<sub>3</sub>O<sub>4</sub>/C was detected to be 0.33 V, whereas it was 0.14 V for 1-Co<sub>3</sub>O<sub>4</sub>/C and 3-Co<sub>3</sub>O<sub>4</sub>/C. The half wave potential of 2-Co<sub>3</sub>O<sub>4</sub>/C is at 0.06 V, while the other two composites give a much more negative half wave potential at -0.1 V. The results from the polarization curves further prove that the 2-Co<sub>3</sub>O<sub>4</sub>/C has higher catalytic activity than two others. To obtain deeper insight into the electron transfer kinetics of mesostructured Co<sub>3</sub>O<sub>4</sub>/C composites during the ORR, typical RDE polarization behaviors of the composites and 40% Pt/C were investigated at different rotating rates (Fig. S3A). The corresponding Koutecky-Levich plots ( $J^{-1}$  vs  $\omega^{-1/2}$ ) of 2-Co<sub>3</sub>O<sub>4</sub>/C at varied electrode potentials show excellent linearities (Fig. 3D), and the slopes remain approximately constant over the potential range from 0 to 0.2 V, indicating a similar electron-transfer number per O<sub>2</sub> molecule involved in the O<sub>2</sub> reduction. The values of  $n$  are around 3.8 in the full range of potential employed, indicating that the ORR process on the obtained 2-Co<sub>3</sub>O<sub>4</sub>/C may undergo a 4e<sup>-</sup> combined pathway.

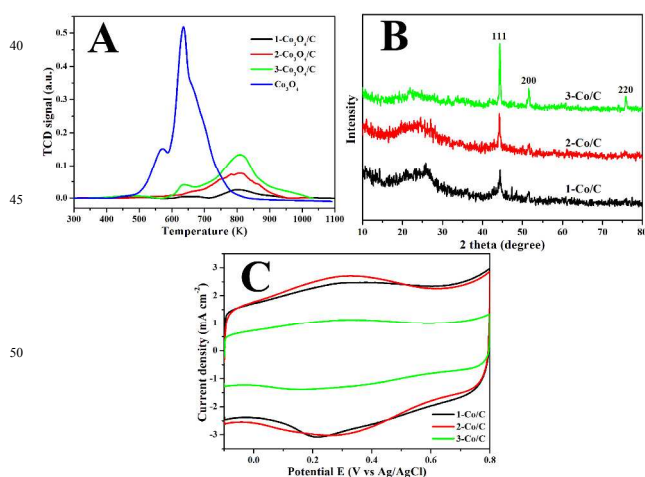
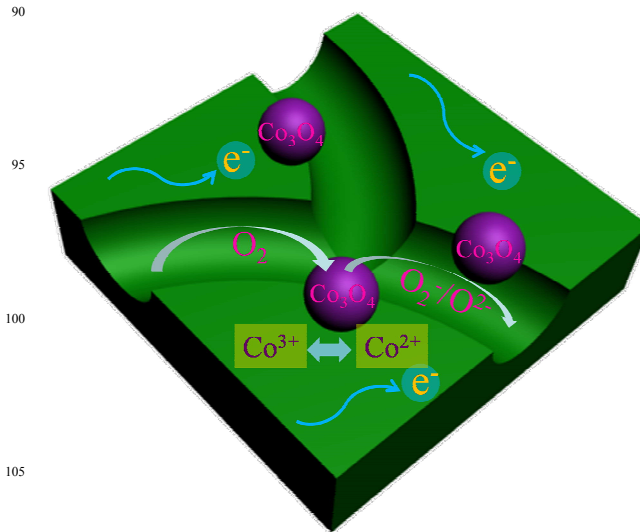


**Fig. 4** H<sub>2</sub>-TPR profiles of the mesostructured Co<sub>3</sub>O<sub>4</sub>/C composites (A); Wide-angle XRD patterns of the mesostructured Co/C composites after heat treatment under 10%H<sub>2</sub>/Ar (B); CV curves of the mesostructured Co/C composites in O<sub>2</sub>-saturated 0.5 M H<sub>2</sub>SO<sub>4</sub>,  $v = 50$  mV s<sup>-1</sup>.

Fig. 4A shows the H<sub>2</sub>-TPR profiles of the mesoporous Co<sub>3</sub>O<sub>4</sub> and mesostructured Co<sub>3</sub>O<sub>4</sub>/C composites. From the H<sub>2</sub>-TPR profile of the mesoporous Co<sub>3</sub>O<sub>4</sub>, two major successive steps were observed at about 573 and 633 K, corresponding to the reductions of Co<sup>3+</sup> to Co<sup>2+</sup>, and Co<sup>2+</sup> to Co<sup>0</sup>, respectively. However, compared with the mesoporous Co<sub>3</sub>O<sub>4</sub>, the two reduction steps of the mesostructured Co<sub>3</sub>O<sub>4</sub>/C composites shift to higher temperatures, and the peak areas become much smaller than that of the pure mesoporous Co<sub>3</sub>O<sub>4</sub>, most probably due to the low crystallinity and low amounts of the Co<sub>3</sub>O<sub>4</sub> nanoparticles highly dispersed in the mesoporous carbon substrates (Fig. 1A, Table S1). As expected, the peak area of the mesostructured Co<sub>3</sub>O<sub>4</sub>/C composites increases gradually from 1-Co<sub>3</sub>O<sub>4</sub>/C to 3-Co<sub>3</sub>O<sub>4</sub>/C, attributing to the increased Co<sub>3</sub>O<sub>4</sub> contents. To confirm the total reduction of Co<sub>3</sub>O<sub>4</sub> to Co, XRD patterns of the samples after H<sub>2</sub>-TPR tests were recorded (Fig. 4B), and the results clearly shows the XRD patterns of metal Co peaks at  $2\theta = 44.2^\circ$ ,  $51.5^\circ$  and  $75.9^\circ$ , corresponding to (111), (200) and (220) lattice planes, respectively (JCPDS No.: 15-0806). No other peaks can be observed, indicating that the Co<sub>3</sub>O<sub>4</sub> nanoparticles have been totally reduced to metal Co.

In order to further investigate the electrochemical catalytic activity of the Co<sub>3</sub>O<sub>4</sub>/C, the electrochemical tests of the corresponding mesostructured Co/C composites obtained after H<sub>2</sub> reduction were performed using CV measurements in O<sub>2</sub>-saturated 0.5 M H<sub>2</sub>SO<sub>4</sub>. The CV curves of the Co/C composites with different Co loading contents are given in Fig. 4C. It can be seen that, besides a very weak redox peaks for 1-Co/C, no redox peaks can be detected for other two mesostructured Co/C composites, suggesting that insignificant or negligible electrochemical ORR activities of the Co/C samples.



**Scheme 1** Schematic illustration of mesostructured Co<sub>3</sub>O<sub>4</sub>/C composites for oxygen reduction. The mesoporous carbon substrates act as the electron transferred media and provide a channel for the diffusion of ORR related species and the enhancement of the catalytic activity. O<sub>2</sub> molecules diffused to the surface of Co<sub>3</sub>O<sub>4</sub>, are decomposed into O<sub>2</sub><sup>-</sup>/O<sub>2</sub><sup>2-</sup> species by means of the Co<sup>3+</sup>/Co<sup>2+</sup> redox couple.

According to the electrochemical ORR properties of the mesoporous Co<sub>3</sub>O<sub>4</sub> and carbon, mesostructured Co<sub>3</sub>O<sub>4</sub>/C and

Co/C composites, it is understood that Co<sub>3</sub>O<sub>4</sub> should be the active species responsible for the electrochemical activity for oxygen reduction. To make a clear understanding of the mesostructured Co<sub>3</sub>O<sub>4</sub>/C composites for oxygen reduction process, a possible mechanism is proposed for the oxygen reduction by mesostructured Co<sub>3</sub>O<sub>4</sub>/C composites as shown schematically in Scheme 1. On one hand, the conductivity of the carbon substrate can provide electron transfer channels to compensate for the weak conductivity of Co<sub>3</sub>O<sub>4</sub> nanoparticles. On the other hand, the relatively high catalytic activity for ORR of the mesostructured Co<sub>3</sub>O<sub>4</sub>/C composite compared with the corresponding Co/C indicates that the Co<sub>3</sub>O<sub>4</sub> nanoparticles as the main active species play an important role in oxygen reduction. The relatively high catalytic activity of mesostructured Co<sub>3</sub>O<sub>4</sub>/C may be attributed to the Co<sup>3+</sup>/Co<sup>2+</sup> redox couples, by means of which the O<sub>2</sub> molecules are decomposed into O<sub>2</sub><sup>-</sup>/O<sup>2-</sup> species. Additionally, the pore framework of the mesoporous carbon may benefit the diffusions of ORR related species and the enhancement of the catalytic activity.

## Conclusions

In summary, the mesostructured Co<sub>3</sub>O<sub>4</sub>/C composites with Co<sub>3</sub>O<sub>4</sub> nanoparticles homogeneously dispersed into mesoporous carbon substrate, are applicable noble metal-free catalytic candidates for oxygen reduction with relatively high catalytic activity and durability. 2-Co<sub>3</sub>O<sub>4</sub>/C with a Co loading content of 4.3 at% shows the highest electrochemical activity, and a 4e<sup>-</sup> process is proposed as the main pathway for oxygen reduction. Moreover, the relatively high catalytic activity of the mesostructured Co<sub>3</sub>O<sub>4</sub>/C composites is mainly attributed to the redox couples (Co<sup>3+</sup>/Co<sup>2+</sup>) in Co<sub>3</sub>O<sub>4</sub> nanoparticles, high conductivity of the carbon substrate and the mesoporous diffusion channels offered by the mesostructure of the composite catalysts for the ORR-related species.

## Notes and references

<sup>a</sup> Key Laboratory for Ultrafine Materials of Ministry of Education, School of Materials Science and Engineering, East China University of Science and Technology, Shanghai 200237, China. E-mail: ysli@ecust.edu.cn

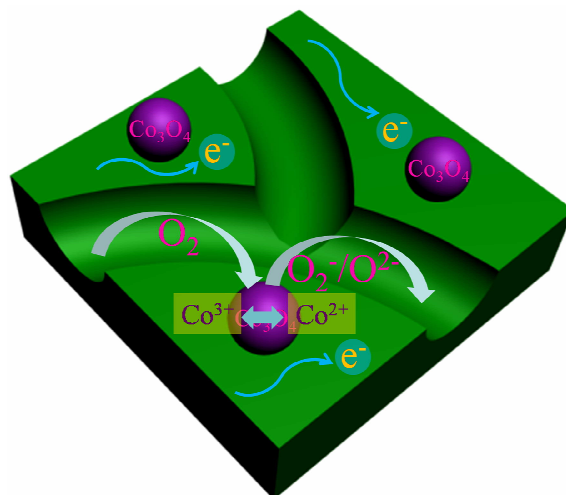
<sup>b</sup> The State Key Laboratory of High Performance Ceramics and Superfine Microstructures, Shanghai Institute of Ceramics, Chinese Academy of Sciences, Shanghai 200050, China. Fax: +86 21 52413122; Tel: +86 21 52412712; E-mail: jlshi@mail.sic.ac.cn

<sup>c</sup> Qian Xuesen Laboratory of Space Technology, China Academy of Space Technology, Beijing 100094, China

† Electronic Supplementary Information (ESI) available: [Pore structure parameters, XPS, CV curves, RDE voltammetry curves]. See DOI: 10.1039/b000000x/

- 1 Y. Nabaie, I. Yamanaka and K. Otsuka, *Appl. Catal. A: Gen.*, 2005, **280**, 149.
- 2 G. Liu, X. G. Li, P. Ganesan and B. N. Popov, *Appl. Catal. B: Environ.*, 2009, **93**, 156.
- 3 Y. J. Feng, N. Alonso-Vante, *Phys. Status Solidi B*, 2008, **245**, 1792.
- 4 R. Bashyam, P. Zelenay, *Nature* 2006, **443**, 63.
- 5 M. Lefèvre, E. Proietti, F. Jaouen and J.-P. Dodelet, *Science*, 2009, **324**, 71.
- 6 C. W. B. Bezerra, L. Zhang, K. C. Lee, H. S. Liu, A. L. B. Marques, E. P. Marques, H. J. Wang and J. J. Zhang, *Electrochim. Acta*, 2008, **53**, 4937.
- 7 Z. Liu, H. Nie, Z. Yang, J. Zhang, Z. Jin, Y. Lu, Z. Xiao and S. Huang, *Nanoscale*, 2003, **5**, 3283.

- 8 L. Yang, S. Jiang, Y. Zhao, L. Zhu, S. Chen, X. Wang, Q. Wu, J. Ma, Y. Ma and Z. Hu, *Angew. Chem. Int. Ed. Engl.*, 2011, **50**, 7132.
- 9 Y. Gorlin and T. F. Jaramillo, *J. Am. Chem. Soc.*, 2010, **132**, 13612.
- 10 Z. S. Wu, S. B. Yang, Y. Sun, K. Parvez, X. L. Feng and K. Müllen, *J. Am. Chem. Soc.*, 2012, **134**, 9082.
- 11 D. S. Geng, H. Liu, Y. G. Chen, R. Y. Li, X. L. Sun, S. Y. Ye, S. Knights, *J. Power Sources*, 2011, **196**, 1795.
- 12 K. Parvez, S. B. Yang, Y. Hernandez, A. Winter, A. Turchanin, X. L. Feng and K. Müllen, *ACS Nano*, 2012, **6**, 9541.
- 13 X. Y. Yan, X. L. Tong, Y. F. Zhang, X. D. Han, Y. Y. Wang, G. Q. Jin, Y. Qin and X. Y. Guo, *Chem. Commun.*, 2012, **48**, 1892.
- 14 Y. Wang, X. J. Lu, Y. Liu and Y. Q. Deng, *Electrochem. Commun.*, 2013, **31**, 108.
- 15 F. Q. Kong, *Electrochim. Acta*, 2012, **68**, 198.
- 16 J. B. Xu, P. Gao and T. S. Zhao, *Energy Environ. Sci.*, 2012, **5**, 5333.
- 17 A. Restovic, E. Ríos, S. Barbato, J. Ortiz and J. L. Gautier, *J. Electroanal. Chem.*, 2002, **522**, 141.
- 18 Y. Y. Liang, Y. G. Li, H. L. Wang, J. G. Zhou, J. Wang, T. Regier and H. J. Dai, *Nature Mat.*, 2011, **10**, 780.
- 19 J. B. Xu, P. Gao and T. S. Zhao, *Energy Environ. Sci.*, 2012, **5**, 5333.
- 20 A. L. M. Reddy, M. M. Shaijumon, S. R. Gowda and P. M. Ajayan, *Nano Lett.*, 2009, **9**, 1002.
- 21 H. Wang, R. Côté, G. Faubert, D. Guay and J. P. Dodelet, *J. Phys. Chem. B*, 1999, **103**, 2042.
- 22 Z. X. Wu, Y. Y. Lv, Y. Y. Xia, P. A. Webley and D. Y. Zhao, *J. Am. Chem. Soc.*, 2012, **134**, 2236.
- 23 J. Zhang, J.-O. Müller, W. Q. Zheng, D. Wang, D. S. S. and R. Schlögl, *Nano Lett.*, 2008, **8**, 2738.
- 24 X. Z. Cui, J. L. Shi, L. X. Zhang, M. L. Ruan and J. H. Gao, *Carbon*, 2009, **47**, 186.
- 25 Q. J. He, J. L. Shi, F. Chen, M. Zhu and L. X. Zhang, *Biomaterials*, 2010, **31**, 3335.
- 26 Z. L. Hua, J. Zhou and J. L. Shi, *Chem. Commun.*, 2011, **47**, 10536.
- 27 Y. S. Li, Y. Chen, L. Li, J. L. Gu, W. R. Zhao, L. Li and J. L. Shi, *Appl. Catal. A: Gen.*, 2009, **366**, 57.
- 28 J. L. Shi, *Chem. Rev.*, 2013, **113**, 2139.
- 29 Z. S. Wu, W. C. Ren, L. Wen, L. B. Gao, J. P. Zhao, Z. P. Chen, Gu. M. Zhou, F. Li and H. M. Cheng, *ACS Nano*, 2010, **4**, 3187.
- 30 J. Feng, Y. Y. Liang, H. L. Wang, Y. G. Li, B. Zhang and J. G. Zhou, *Nano Research*, 2012, **5**, 718.
- 31 Y. Wang, X. J. Lu, Y. Liu and Y. Q. Deng, *Electrochem. Commun.*, 2013, **31**, 108.
- 32 F. Kleitz, S. H. Choi and R. Ryoo, *Chem. Commun.*, 2003, **39**, 2136.
- 33 J. Sauer, F. Marlow, B. Spliethoff and F. Schüth, *Chem. Mater.*, 2002, **14**, 217.
- 34 H. Vidal, S. Bernal, R. T. Baker, D. Finol, J. A. Pérez Omil, J. M. Pintado and J. M. Rodríguez-Izquierdo, *J. Catal.*, 1999, **183**, 53.
- 35 M. R. Gao, Q. Gao, J. Jiang, C. H. Cui, W. T. Yao, and S. H. Yu, *Angew. Chem. Int. Ed.*, 2011, **50**, 4905.
- 36 Y. J. Feng, T. He and N. Alonso-Vante, *Chem. Mater.*, 2008, **20**, 26.



The mesoporous carbon substrates act as the electron transferred media and provide a channel for the diffusion of ORR related species.  $\text{O}_2$  molecules diffused to the surface of  $\text{Co}_3\text{O}_4$ , are decomposed into  $\text{O}_2^-/\text{O}^{2-}$  species by means of the  $\text{Co}^{3+}/\text{Co}^{2+}$  redox couple.